Fatigue response of additively manufactured as-built 15-5 PH stainless steel and effects of machining and thermal and surface treatments

FATIGUE RESPONSE OF ADDITIVELY MANUFACTURED AS-BUILT 15-5 PH STAINLESS STEEL AND EFFECTS OF MACHINING, THERMAL AND SURFACE TREATMENTS

Dario Croccolo [1], Nebojša Bogojević [2], Massimiliano De Agostinis [1], Stefano Fini [1], Giorgio Olmi [1], Francesco Robusto [1], Zlatan Šoškić [2], Snežana Ćirić-Kostić [2]

[1] Department of Industrial Engineering (DIN), University of Bologna, Bologna, Italy

[2] Faculty of Mechanical and Civil Engineering in Kraljevo, University of Kragujevac, Serbia

Corresponding Author:
Prof. Giorgio Olmi
Department of Industrial Engineering (DIN)
University of Bologna
Italy
E - mail: giorgio.olmi@unibo.it

ABSTRACT

Additively produced 15-5 PH Stainless Steel has wide industrial applications, but the combined effects of heat treatment, machining and shot-peening and their order have not been deeply investigated. This topic is addressed here by a 2-by-3 experimental plan that has involved S-N curve and fatigue limit determination, using vertically built cylindrical samples, tested under rotating bending. The obtained responses have been analysed by an ANOVA-based statistical approach for comparison of fatigue trends. Results indicate that heat treatment without machining may be even detrimental for fatigue due to embrittlement. Conversely, machining with subsequent shot-peening, even without heat treatment, has a remarkable impact and leads to a doubled fatigue strength with respect to as-built material. This strength is also quite close to that achievable for wrought material. The study has been completed by micrography and fractography, to reveal the dependence of microstructure, crack initiation sites and failure mode on the performed treatments.

Keywords: fatigue; powder bed fusion; 15-5 Stainless Steel; heat treatment; machining; shot-peening.

NOMENCLATURE

AM	Additive Manufacturing
ANOVA	Analysis of Variance
b_0, b_1	S-N curve coefficients according to ISO 12107 Standard
DMLS	Direct Metal Laser Sintering

FL	Fatigue limit (or strength) at 10 million cycles
k	Confidence-related tabled coefficient from ISO 12107 Standard
MLE	Maximum likelihood estimation
PBF	Powder Bed Fusion
N	Lifecycles (for S-N curve)
R	Stress Ratio (fatigue tests)
R_a	Roughness Average [μm]
$\overline{S_{1.}}, \overline{S_{2.}}$	Row means (for ANOVA computations)
$\overline{S_{.1}}, \overline{S_{.2}}, \overline{S_{.3}}$	Column means (for ANOVA computations)
$\overline{S_{..}}$	Overall mean (for ANOVA computations)
SLM	Selective Laser Melting
S	Maximum Bending Stress (for S-N curve)
S_{HMP}	10-base logarithm of stress, for Set HMP (for ANOVA computations)
S_{MP}	10-base logarithm of stress, for Set MP (for ANOVA computations)
S_P	10-base logarithm of stress, for Set P (for ANOVA computations)
S_{PH}	10-base logarithm of stress, for Set PH (for ANOVA computations)
S_{PHM}	10-base logarithm of stress, for Set PHM (for ANOVA computations)
S_{PM}	10-base logarithm of stress, for Set PM (for ANOVA computations)
S-N curve	Maximum Bending Stress vs. Life Cycles curve in the finite life domain
SSBC', SSBC	Sum of Squares between Columns (for ANOVA computations, for a generic life N and integral mean over the considered lifespan)
SSE	Sum of Squares Error, taking experimental scattering into account (for ANOVA computations)
SSI', SSI	Sum of Squares Interaction (for ANOVA computations, for a generic life N and integral mean over the considered lifespan)
SSBR', SSBR	Sum of Squares between Rows (for ANOVA computations, for a generic life N and integral mean over the considered lifespan)

UTS	Ultimate Tensile Strength [MPa]
YP	Yield Point [MPa]
σ	Standard deviation of the S-N curve linear regression according to ISO 12107 Standard

1. INTRODUCTION

Over the latest 35 years, after the invention of the first machine for Additive Manufacturing (*AM*), there has been great progress in this field. The key point in development of *AM* technologies for metal processing is to achieve mechanical properties, in particular fatigue resistance, of parts comparable to those of wrought material. A further point regards eco-sustainability of the AM technologies. On one hand [1-2], *AM* brings benefit of reducing the amount of raw material needed for the process. On the other hand [3], some issues have been raised regarding energy consumption at particular stages of the process. Indeed, *AM* makes it possible to produce complex geometries as single components and also to pursue a high strength-to-weight ratio goal. However, this point again calls for an accurate comprehension regarding mechanical response. A further aspect of *AM* technologies being relevant for this paper is post-processing treatment of products: heat treatments may enhance the material properties, but imply a longer production time, causing additional costs and a substantial increase of energy consumption. On the other hand, surface treatments may be more energy efficient.

Powder Bed Fusion (*PBF*) is a family of Additive Manufacturing (*AM*) technologies for direct manufacturing of products from metal and plastic materials. A common *PBF* technology for metal processing is Direct Metal Laser Sintering (*DMLS*), also known as Selective Laser Melting (*SLM*). The technology can be applied to a variety of metal alloys, such as maraging and stainless steels, aluminium, titanium, copper alloys [4].

The most popular stainless steels for DMLS include 316L, 17-4 PH, CX and 15-5 PH. The first one is classified as an Austenitic stainless steel and exhibits a very good corrosion and acid resistance, which makes it a valid candidate for applications in aerospace, oil & gas, nuclear power plants and bioengineering [4-9].

Precipitation hardening stainless steels are generally martensitic and their main feature is the so-called precipitate strengthening behaviour. Carbide precipitation, which has conversely a detrimental effect, is limited by the low C concentration, whereas a moderate amount of Ni is present [10]. Tool manufacturing may be regarded as their main application field.

Stainless steel CX can be regarded as a recently introduced Maraging Stainless steel, featuring a low carbon content and a high amount of chromium. Previous studies have indicated it exhibits a remarkable corrosion resistance, together with high hardness and good static properties. This alloy takes advantage of the precipitation of the β-NiAl intermetallic phase [11]. Recent studies have indicated it is suitable for injection moulding tools even in harsh environments [12]. Moreover, it can be applied for shipbuilding, in oil & gas, in offshore technologies and nuclear power plants [13]. Most papers [12, 14-15] are focused on the static response and on the microstructure and the achievable metallurgical properties, following different heat treatments. A previous study by the authors of this paper [16] has been devoted to the investigation of the fatigue response of this material, assessing the effects of heat treatment and machining. It has been concluded that the effect of machining appears to be stronger than that of heat-treatment by annealing and aging. Machining, making the external surface smoother and removing potential nucleation sites, leads to a fatigue limit close to 40% of the corresponding ultimate tensile strength.

17-4 PH Stainless Steel is widely used in *AM*, in order to take advantage of its good printability, good strength and corrosion resistance. These properties make it suitable for surgical instruments [17-19]. Due to its wide application, a lot of studies dealing with static and fatigue properties are already available in the scientific literature [20-21].

Conversely, 15-5 PH Stainless Steel is more rarely studied, despite interesting properties from the points of view of static strength, toughness and corrosion resistance at both room and high temperatures, especially in the precipitation hardened state. The material can be utilized for functional prototypes and serial production of parts such as valves, shafts, fasteners and gears [22-24]. However, the microstructures of wrought 15-5 PH and 15-5 PH obtained by DMLS have some differences: in particular, martensite laths keep longer and wider for wrought material [25]. The stacking process leads to higher ultimate tensile strength (*UTS*), but to more brittle features [25-26]. A further study [27] indicates that the 15-5 PH Stainless Steel produced by *DMLS* and post-processed by subsequent age hardening exhibits enhanced yield strength regardless of part orientation, whereas fracture toughness remains comparable to that of wrought material. However, it must be remarked that the available studies in the literature mainly deal with static properties [24, 28-32]. Conversely, there are few studies on the fatigue response of 15-5 PH Stainless Steel in the literature. Ref. [33] is focused on additively processed 15-5 PH Stainless Steel under low and high cycle fatigue. This research has investigated the effects of aging and over-aging treatment, revealing that the aging (H900) treatment has beneficial effects on static properties due to precipitation hardening strengthening of material matrix. Conversely, material is made more brittle under fatigue [33-34] and appears to be notch-sensitive in the as-built conditions. However, the effects of machining and surface treatment, in particular, shot-peening, and their

combined effects with heat treatment are not investigated. Mechanical behaviour under cyclic loading is usually regarded as a drawback of additively processed materials [26, 35]. In particular, surface defects or roughness irregularities in the unmachined state are likely to detrimentally affect the fatigue strength [36]. A previous study by the authors of this paper [37] has also been focused on the fatigue response of 15-5 PH, investigating the effects of build orientation and of allowance for machining, and involving machined and heat-treated samples. The obtained results indicate that the fatigue limit for infinite life is generally significantly lower 50% of the *UTS*, which is the commonly accepted value for wrought metallic materials. However, it can be improved by slanted orientation of the longitudinal axis of the samples with respect to the stacking direction, as layer orientation acts as barrier against crack propagation. In addition, a further enhancement may arise from machining parts from oversized blocks, that is to say from adopting a larger allowance. In this case, defects at the surface or just beneath it may be removed, which contributes to an enhancement of the fatigue response. This outcome also confirms that most relevant detrimental factor must be attributed to defects, such as voids, located on the surface or just beneath it.

Some aspects concerning the fatigue response of materials produced by *AM* have been the topic of other papers by the authors [37-40]. In particular, studies on Maraging Steel MS1 [40] have revealed that the fatigue response of this material may be particularly incremented by applying shot-peening after machining, even without heat-treatment. This surface treatment is usually applied immediately after the *AM* production process, to close the surface porosities and to build up a beneficial compressive residual stress state. The previous study on CX [16] has also confirmed that running shot-peening after machining is highly beneficial to fatigue resistance of the material.

Resuming the remarks above, 15-5 PH fatigue response has been rarely studied despite the many applications under cyclic loads of this material. Moreover, the fatigue response is highly affected by surface roughness conditions and by surface or subsurface defects. It is worth mentioning that in many applications with complex geometries it is not possible to perform machining and, therefore, the part must operate in the as-built state. A literature survey indicates a lack of studies addressing fatigue of this material with and without machining. A further point is related to shot-peening after machining that proved to be beneficial on Maraging Steel and on CX, but an insight comparative study has not been conducted on 15-5 PH. This paper addresses these issues from the experimental point of view, taking also heat-treatment into account. The novelty of the present study is concerned with the implementation of a factorial plane addressing the combined effects of heat-treatment, machining and shot-peening and related order. In the framework of this factorial plane, data regarding the fatigue response in the unmachined condition have been determined as well. Statistical

assessments have been run to compare the performance in different conditions and microscope observations have completed the study.

2. MATERIALS AND METHODS

The material used in the present study was Stainless Steel PH1, which is considered to be a 15-5 PH Stainless Steel. Material powder was supplied by EOSGmbH – Electro Optical Systems, Krailling/Munich, Germany that provided certification for the chemical composition, with reference to wt%, as reported in Table 1. Fresh (not recycled) powder was used in the production process.

Table 1: Chemical composition of 15-5 PH Stainless Steel (wt%)

Cr [%]	Ni [%]	Cu [%]	Mn [%]	Si [%]	Mo [%]	Nb [%]	C [%]	Fe [%]
14-15.5	3.5-5.5	2.5-4.5	≤1	≤1	≤0.5	0.15-0.45	≤0.07	Bal.

The final geometry of the samples used in this study was compliant with the requests of the ISO 1143 [41] Standard that described fatigue tests under rotary bending, with 6mm diameter at gage (20.4mm long), 10 mm diameter at the heads, and 25mm fillet radius. A sample drawing is depicted in Fig. 1.

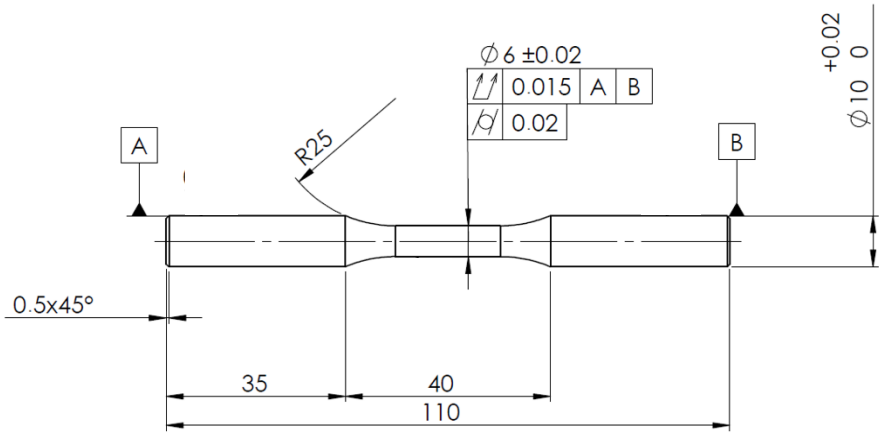

Fig. 1: Sample geometry in agreement with ISO 1143 Standard [41] (all dimensions in mm)

All the samples in this study were built by *DMLS* technology using an EOSINT M280 machine (by EOS GmbH - Electro Optical Systems, Krailling/Munich, Germany) operating with an infrared Ytterbium fibre laser with 1,064 nm wavelength and maximal power 200W. The laser beam had

thickness of 0.2032 mm and a maximum scanning speed up to 7,000 mm/s. The manufacturing process was run in a nitrogen atmosphere within the production chamber with baseplate dimensions 250 mm × 250 mm and with height 325 mm. Process parameters were selected complying with EOS Part Property Profile named "Surface", which is optimized for optimal surface quality of products, and comprises layer thickness 20 μm and alternated parallel scan strategy with 70° rotation between adjacent layers. All the samples were built in a single AM production process (one batch) with vertical orientation of their main axis of inertia during the manufacturing process.

The experimental campaign involved two factors: the first describes post-processing by heat-treatment and the second machining and surface treatment by shot-peening. The assessment of their effects and interactions was addressed by the two-factor design reported in Table 2, where heat-treatment is regarded as the row-factor, whereas the machining and surface treatment is the column-factor. Implementation of the two-factor design comprised manufacturing of six different sample sets, and each of the sets consisted of 15-16 samples.

Table 2: Design of the experimental campaign with sample set identifiers

		Surface treatment		
		Shot-peening only	**Shot-peening with subsequent machining**	**Machining with subsequent shot-peening**
Heat Treatment	No	P	PM	MP
	Yes	PH	PHM	HMP

The first factor, heat-treatment, was implemented as on-off variable, meaning that three sample sets were not heat-treated, whereas the other three were heat-treated according to the following recipe: samples were heated, following a linear increase from room temperature to 482°C in one hour-time. Afterwards, they were kept at this temperature for 2 hours; a slow cooling to room temperature was finally run in a furnace. This treatment, commonly known as H900, is recommended by the supplier [37, 42] and is aimed at reducing stacking process-induced tensile residual stresses and at promoting precipitation hardening, also optimizing part density. According to [42], heat treatment has also the capability of enhancing static properties: the *UTS* is increased from 1,050 to 1,310MPa, whereas the Yield Point (*YP*) is incremented from 1,000 to 1,170MPa. The other factor involved three levels: the first one corresponds to just a basic shot-peening treatment by stainless steel shots with 0.7mm average diameter under a 5 bar airstream pressure. During the shot-peening, the airstream was kept

normal to the treated surface at a distance of approximately 50 mm. The second level corresponds to shot-peening (as described above) with subsequent machining by turning and grinding with 0.5 mm allowance. The third level was similar to the previous one, with the difference being that the order of two post-processing treatments was changed: machining was performed before shot-peening. The rationale for testing the fatigue response under this condition was to prevent removal of the surface layer treated by shot-peening during the subsequent machining, as suggested by previous studies on other materials. In fact, shot-peening commonly induces effects in terms of pore closure and of beneficial compressive residual stresses (that counterbalance the tensile ones induced by the *DMLS* process) up to a depth of about 0.1 mm. Therefore, running machining with 0.5 mm (or, frequently, higher) allowance leads to the complete removal of that treated layer, where compressive stresses are present. Conversely, swapping the treatments makes it possible to significantly smoothen the surface, while, at the same time, taking advantage of the built up beneficial residual stress distribution. Shot-peening is likely to lead to a incremented roughness (up to around 1μm), but the positive outcomes are expected to be prevalent, as observed for other materials [16, 40].

It is worth mentioning that it is usually highly recommended to perform heat-treatment while the samples are still attached to the baseplate. In fact, significant tensile residual stresses are generated during the stacking process: keeping the samples connected to the baseplate until the heat-treatment is run prevents the residual stress state from generating unacceptable deformations, as highlighted in [37]. Following heat-treatment execution, residual stresses are dropped down and therefore samples may be safely detached without inconvenience. In addition, it is clear the sample detachment must always precede machining.

These remarks in the previous paragraph have, therefore, affected the reported procedure concerning the order of post-processing treatments for the six sample sets in Table 2. The samples of Set P underwent just shot-peening after building by DMLS, while being still attached to the baseplate. The samples of Set PH underwent the same shot-peening treatment and were afterwards heat-treated by the H900 procedure (while being still attached to the baseplate). Similarly, the samples from Set PM were first shot-peened; afterwards, they were detached from the baseplate and then machined. The samples included in Set PHM were shot-peened, heat-treated and detached from the baseplate and finally machined. The samples from Set MP were detached immediately after the additive process, machined and shot-peened. Finally, the samples included in Set HMP were heat-treated, detached, machined and then shot-peened. It may be argued other possible combinations may be available: in particular, involving a swapped order between shot-peening and heat-treatment, when these treatments are run before machining. However, running heat-treatment before shot-peening increases surface hardness, which would reduce the beneficial effects related to shot impacts in terms, for

instance, of pore closure. On the other hand, running heat treatment after machining would be completely unfeasible, as it would require immediate detachment from baseplate with consequent significant deformation largely beyond specifications. This distortion could not be reasonably fixed by subsequent machining.

3. EXPERIMENTAL

Prior to experimental testing, all the samples underwent dimensional and roughness checks, both at gages and at the heads, with a sufficient number of replications for statistical evidence reasons. In particular, dimensional and roughness measurements at gages were performed with six and eight replications, respectively. All the samples appeared to be compliant with dimensional specifications and tolerance ranges requested by Standard ISO 1143 [41]. As for roughness, averaged R_a values were 6.4μm for unmachined samples (Sets P and PH) and 0.6μm for peened and machined ones (Sets PM and PHM). As expected, when run after machining (Sets MP and HMP), the shot-peening treatment led to an increase of roughness up to 0.8μm, as an effect of impact-related dimples. Rockwell hardness was measured as well, complying with [43]: related results, averagely 33 HRC for untreated and 41 HRC for treated sets are well aligned with the specifications in the material datasheet by EOS [42]. Hardness levels were consistent for all the heat-treated samples, regardless of final peening treatment.

In addition, in order to ensure agreement with supplier specifications, densities of all the samples were measured by an electronic balance under the application of the Archimedes' thrust immersion method. Relative density was finally computed, normalizing the determined density with respect to the related nominal value, 7,800 kg/m^3, based on the material datasheet by EOS [42]. All the measurements were run with three repetitions per sample for the sake of statistical evidence. The obtained relative densities, ranging between 99.0 and 99.5% for the six sample sets, are well aligned with the specifications by the supplier, and prove to be independent of the performed heat and surface treatments.

The tests under rotating bending were aimed at the determination of the S-N curves in the finite life domain and of the fatigue limits for infinite life. Test were run by an electrically actuated four-point rotating bending machine (RB 35, by Italsigma, Forlì, Italy) with constant maximum moment at gage with Stress Ratio R=-1 at the frequency f=60Hz. This machine operates under load control. Therefore, based on bending moment constant distribution and on the measurement of the actual diameter at gage, maximum bending stress level is also accurately controlled. Load levels were set, based on the desired stress levels that are provided in Table 3. Failure criterion was sample complete separation,

which led to automatic trial interruption. A 10 million cycles run-out value was set, based on recommendations from [37]. The S-N curves were processed by two methods. They were initially determined, following the procedure described in Standard ISO 12107 [44], including the determination of confidence bands for 10 and 90% probabilities of failure and 90% confidence level. Before proceeding to fatigue limit determination, the fatigue data were also processed by a "Maximum Likelihood Estimation (MLE)" approach. This procedure made it possible to determine S-N curve trends, accounting for both complete (failures) and censoring data (runouts). As a consequence, both the sloping part (for high stress levels) and the curvature (in the neighbourhood of the fatigue limit) could be suitably modelled. This method was initially developed by [45] and is based on the maximization of a logarithmic likelihood function. The S-N curve at the desired probability of failure may subsequently be worked out [46-49]. The fatigue limits were determined based on the failure – not-failure sequences, following the Dixon method, which is to be regarded as an abbreviated staircase testing procedure involving 8 to 10 nominal samples [37, 50-53]. Fatigue limit confidence bands at the 90% confidence level, taking both data scattering (variance) and sequence size into account, were determined as well. Fracture surfaces were then analysed by a stereo-microscope (Stemi 305, by ZEISS, Oberkochen, Germany), to individuate crack nucleation sites, investigating their locations and crack triggers. At a following stage, fracture surface analysis was deepened with the aid of a hot-cathode Field Emission Gun (FEG) Scanning electron microscope (SEM) that is equipped with secondary electron detector, wobble adjustment and stigmator alignment for high resolution imaging (Mira3 Model, by TESCAN, Brno, Czech Republic). This tool was utilized, to investigate defects at initiation points, fatigue propagation lines and fracture ductility or brittleness features upon final separation. Micrographic studies were also run to assess the layered structure arising from the additive process and how it is affected by heat-treatment. For this purpose, resin-embedded samples underwent a chemical etching by Vilella's reagent with surface pre-heating. In particular, surface was pre-heated up to 300°C by a hot airstream for 30 s. Vilella etchant was then applied for just a few seconds before sample drying by a blow of compressed air. Afterwards, observations of resin-embedded samples were carried out by an optical microscope (Optiphot-100, by Nikon, Melville, NY, United States).

4. RESULTS AND DISCUSSION

4.1 Results

The results of the fatigue testing campaign are collected in Table 3. All of them were processed by linear regressions complying with [44], following the application of the general linear test, according to

Eq. (1) and Eq. (2). Upper and lower bounds were determined as well, according to Eq. (3). The calculated coefficients b_0 and b_1 are provided in Table 4.

$$Log(N) = b_0 - b_1 \cdot Log(S) \quad (1)$$

$$S = 10^{\frac{b_0}{b_1}} \cdot N^{-\frac{1}{b_1}} \quad (2)$$

$$Log(N) = b_0 - b_1 \cdot Log(S) \pm k \cdot \sigma \quad (3)$$

Table 3: Results of the fatigue campaign under rotary bending (excluding outliers)

Specimen Set	Stress amplitude [MPa]	Cycles to Failure	Failure / Run-out
P	490	61,447	Failure
P	430	49,597	Failure
P	370	128,377	Failure
P	310	113,581	Failure
P	230	---	Run-out
P	250	311,432	Failure
P	190	---	Run-out
P	250	848,241	Failure
P	230	239,198	Failure
P	210	514,624	Failure
P	210	---	Run-out
P	310	214,627	Failure
P	370	191,471	Failure
P	430	83,400	Failure
PH	430	31,955	Failure
PH	370	48,038	Failure
PH	250	134,936	Failure
PH	190	453,024	Failure
PH	150	---	Run-out
PH	170	---	Run-out
PH	190	---	Run-out
PH	210	---	Run-out
PH	230	430,937	Failure

PH	210	---	Run-out
PH	250	336,160	Failure
PH	370	76,975	Failure
PH	310	79,475	Failure
PH	310	97,653	Failure
PM	330	7,580,782	Failure
PM	370	1,739,870	Failure
PM	330	1,698,064	Failure
PM	310	---	Run-out
PM	330	---	Run-out
PM	490	130,951	Failure
PM	390	---	Run-out
PM	430	278,836	Failure
PM	310	---	Run-out
PM	350	---	Run-out
PM	470	108,863	Failure
PM	470	78,805	Failure
PM	450	---	Run-out
PM	450	272,910	Failure
PM	490	57,925	Failure
PM	430	---	Run-out
PHM	610	104,918	Failure
PHM	490	210,854	Failure
PHM	550	40,802	Failure
PHM	430	5,440,374	Failure
PHM	400	---	Run-out
PHM	430	9,014,603	Failure
PHM	414	1,297,328	Failure
PHM	400	---	Run-out
PHM	430	1.402,715	Failure
PHM	400	---	Run-out
MP	490	4,774,345	Failure
MP	450	1,169,313	Failure
MP	410	---	Run-out
MP	430	---	Run-out

MP	530	35,788	Failure
MP	510	446,099	Failure
MP	530	151,062	Failure
MP	510	542,286	Failure
MP	430	---	Run-out
MP	450	---	Run-out
MP	470	---	Run-out
MP	550	186,663	Failure
HMP	490	4,263,499	Failure
HMP	450	8,291,561	Failure
HMP	430	---	Run-out
HMP	450	8,208,407	Failure
HMP	430	5,853,868	Failure
HMP	410	---	Run-out
HMP	430	---	Run-out
HMP	530	---	Run-out
HMP	570	6,817,893	Failure
HMP	610	329,363	Failure
HMP	650	81,922	Failure
HMP	610	372,077	Failure
HMP	570	188,516	Failure
HMP	530	339,034	Failure

Table 4: Coefficients of the determined *S*-*N* curves, according to the linear model of ISO 12107 [44]

Set #	b_0	b_1	$10^{b0/b1}$	$-1/b_1$	$k \cdot \sigma$
P	11.910	2.661	29,952	-0.376	0.415
PH	13.593	3.445	8,838	-0.290	0.329
PM	31.451	9.867	1,540	-0.101	0.505
PHM	36.709	11.533	1,524	-0.087	1.278
MP	49.651	16.278	1,123	-0.061	1.361
HMP	33.516	10.066	2,136	-0.099	1.039

The fatigue curves are plotted altogether in Fig. 2 along with experimental data represented by dots. The obtained trends were compared by an *ANOVA*-based extended statistical method for the comparison of fatigue trends. This method was firstly introduced in [54] and then successfully applied [16, 37, 39-40], to carry out a rigorous statistical analysis of the S-N curve trends, involving the effects of two factors, as well as their possible interaction, on the fatigue responses. S-N curves in the finite life domain were determined, considering failure results only, i.e. not censoring data. It seemed to be reasonable to make use of these curves for statistical comparison purposes for consistency reasons with the recommended interpolating procedure by Standard ISO 12107 [44] (where censoring data are not addressed) and with the aforementioned previous studies. Furthermore, as highlighted below, including censoring data in the analysis does not significantly affect the trend of the sloping part of the curve being compared here.

4.2 Statistical analysis

The rationale for this analysis is to compare the differences, namely the distances among the obtained S-N curves to the scattering of the experimental results, which are regarded as a reliable indicator of the experimental uncertainty. All the data have been processed in the logarithmic scale, denoting by S_i the 10-base logarithm of the stress level corresponding to a generic life for the i-th S-N curve. The subscript *i* denotes the identifier of the set the S-N curve refers to. As a first step, the row mean curves and the column mean curves need to be calculated: they are the means of the curves in the rows and in the columns of the experimental plan presented in Table 2. They are here denoted as ($\overline{S_{1.}}$, $\overline{S_{2.}}$) corresponding to the two row-means, and as ($\overline{S_{.1}}$, $\overline{S_{.2}}$, $\overline{S_{.3}}$), corresponding to the three column-means (Eq.s (4) to (8)) and are all functions of the fatigue life *N* within the considered lifespan.

$$\overline{S_{1.}} = \frac{S_P + S_{PM} + S_{MP}}{3} \tag{4}$$

$$\overline{S_{2.}} = \frac{S_{PH} + S_{PHM} + S_{HMP}}{3} \tag{5}$$

$$\overline{S_{.1}} = \frac{S_P + S_{PH}}{2} \tag{6}$$

$$\overline{S_{.2}} = \frac{S_{PM} + S_{PHM}}{2} \tag{7}$$

$$\overline{S_{.3}} = \frac{S_{MP} + S_{HMP}}{2} \tag{8}$$

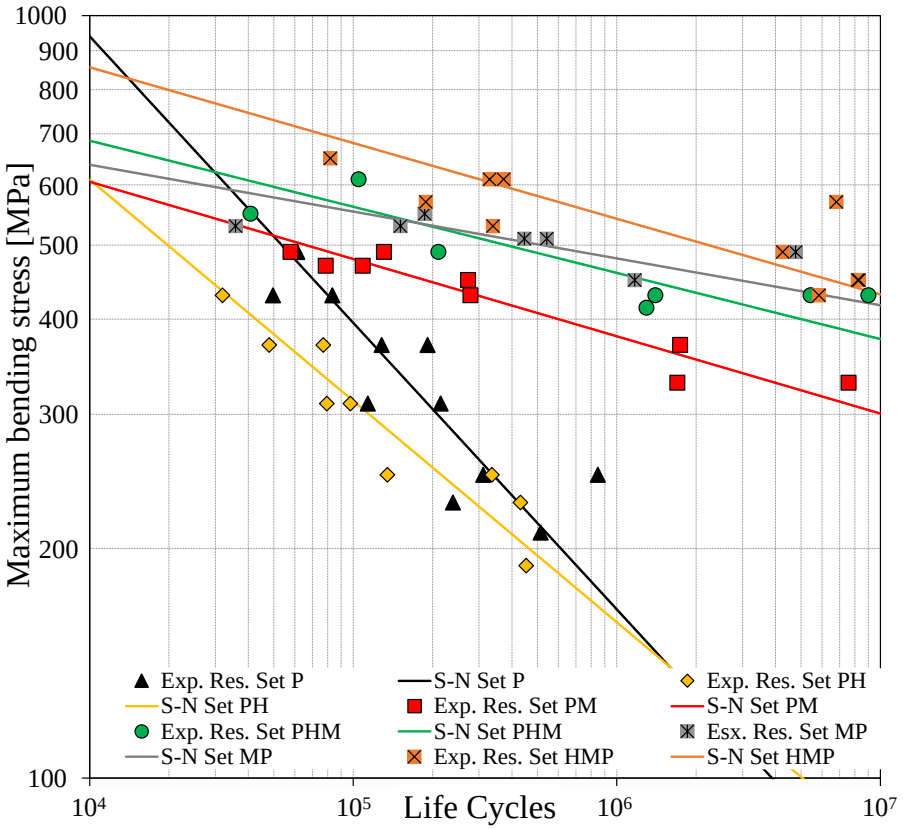

Fig. 2: S-N curves in the finite life domain for the six 15-5 PH Stainless Steel Sets

As a further step, the overall mean $\overline{S_{..}}$, namely the grand-mean, which is also a function of the fatigue life, involving all the curves for the six combinations must be estimated in Eq. (9):

$$\overline{S_{..}} = \frac{S_P + S_{PM} + S_{MP} + S_{PH} + S_{PHM} + S_{HMP}}{6} \tag{9}$$

The "Sum of Squares between Rows" (*SSBR'*) term, related to the effect of the "Row" factor of Table 2, i.e. to the effect of the heat-treatment, was calculated by Eq. (10). This term can be regarded as the sum of the squares of the differences between the row- and the grand-means into account and is weighted by a factor 3, based on the row-means being averaged over three curves.

$$SSBR' = 3\left[\left(\overline{S_{1.}} - \overline{S_{..}}\right)^2 + \left(\overline{S_{2.}} - \overline{S_{..}}\right)^2\right] \tag{10}$$

The "Sum of Squares between Columns", *SSBC'*, is related to the effect of the "Column" factor of Table 2, i.e.: surface treatment. It was similarly computed by Eq. (11) as the sum of the squares of the differences between column- and grand-means. The related weight factor is two, as each column mean is averaged over two curves.

$$SSBC' = 2\left[\left(\overline{S_{.1}} - \overline{S_{..}}\right)^2 + \left(\overline{S_{.2}} - \overline{S_{..}}\right)^2 + \left(\overline{S_{.3}} - \overline{S_{..}}\right)^2\right] \tag{11}$$

Finally, the interaction term *SSI'* is calculated by Eq. (12).

$$SSI' = \left(S_P - \overline{S_{1.}} - \overline{S_{.1}} + \overline{S_{..}}\right)^2 + \left(S_{PM} - \overline{S_{1.}} - \overline{S_{.2}} + \overline{S_{..}}\right)^2 + \left(S_{MP} - \overline{S_{1.}} - \overline{S_{.3}} + \overline{S_{..}}\right)^2 + \\ + \left(S_{PH} - \overline{S_{2.}} - \overline{S_{.1}} + \overline{S_{..}}\right)^2 + \left(S_{PHM} - \overline{S_{2.}} - \overline{S_{.2}} + \overline{S_{..}}\right)^2 + \left(S_{HMP} - \overline{S_{2.}} - \overline{S_{.3}} + \overline{S_{..}}\right)^2 \quad (12)$$

With regard to *SSBR'*, *SSBC'* and *SSI'*, the related functions of the fatigue life within the considered lifespan were turned into scalars by the computation of their integral means over the aforementioned span between 10^4 and 10^7 cycles in the finite life domain of the S-N curves. Related formulas are reported below in Eq.s (13) to (15).

$$SSBR = \frac{1}{Log(10^7) - Log(10^4)} \cdot \int_{Log(10^4)}^{Log(10^7)} SSBR' \; dN \quad (13)$$

$$SSBC = \frac{1}{Log(10^7) - Log(10^4)} \cdot \int_{Log(10^4)}^{Log(10^7)} SSBC' \; dN \quad (14)$$

$$SSI = \frac{1}{Log(10^7) - Log(10^4)} \cdot \int_{Log(10^4)}^{Log(10^7)} SSI' \; dN \quad (15)$$

The term that accounts for experimental uncertainty was finally determined as the sum of the squares of the residuals between the actual experimental data and the analytically predicted ones based on the interpolating curves.

All the data were then processed as a conventional two-factor ANOVA, provided that the sum-of-squares terms had to be scaled, rationalizing them by the respective degrees of freedom. Thus, they were made comparable, which allowed calculation of Fisher's ratios over uncertainty and of and p-values. The latter may be easily computed as the areas of the tails of the corresponding Fisher's statistical distributions, considering portions at the right side with respect to the aforementioned previously computed Fisher's ratios. Its calculation may be easily run by many computational softwares. The p-value retains the meaning of the probability of failing, when concluding that an input factor does significantly affect an observed output. Thus, a very low value indicates that the probability of making an error is also very low, which means there is a great evidence. Conversely, a high value indicates the error probability to be accepted would be too high. Therefore, based on the available data, it cannot be concluded a significant effect is present. A commonly accepted threshold [55-56] is 0.05 (5%): if p-value keeps lower, a significant effect may be inferred. Conversely, if it is greater, the significance of the effect is not proved. The *ANOVA* outcome is displayed in Table 5.

Table 5: ANOVA Table for the two-factor design (lifespan between 10^4 and 10^7)

	Sum of squares	**Degrees of freedom**	**Sum of Squares after scaling**	**Fisher's ratio**	***p-value***
***SSBR*: Effect of the heat treatment**	0.0017	1	0.0017	0.70	0.41
***SSBC*: Effect of surface treatment**	0.0928	2	0.0464	18.60	1.78×10^{-6}
***SSI*: Interaction**	0.0088	2	0.0044	1.76	0.19
***SSE*: Error**	0.1023	41	0.0025		

4.3 Result interpretation

For this class of materials, heat-treatment effect is usually related to precipitation hardening, where Cu-rich precipitates exhibit a strengthening effect, whereas carbide precipitation is suppressed, to prevent corrosion resistance drop [57]. However, the application of the statistical approach described in the previous sub-Section has highlighted that there is not sufficient evidence to reject the so-called "null hypothesis", i.e., based on the retrieved data, heat-treatment does not significantly affect the fatigue strength. On one hand, when considering just shot-peened samples, the heat treatment results in a slight reduction of the fatigue strength, which can be observed, comparing the S-N curves for Sets P and PH. This is due to material being made more brittle and highly notch-sensitive, as also highlighted in [33-34]. This detrimental effect also occurs because heat treatment relaxes the beneficial compressive residual state yielded by shot-peening. On the other hand, heat treatment has a slightly beneficial impact for machined parts (in particular for Set PM vs. PHM), as the strengthening due to precipitation hardening slightly prevails when the external surface is smooth. Therefore, aiming at analysis refinement, the same statistical tool was applied to perform a comparison between S-N curve pairs for the same surface treatment (Sets P vs. PH; PM vs. PHM and MP vs. HMP). The three statistical assessments led to the same consistent conclusion that, based on the here processed and compared data, the effect of the performed heat-treatment is not significant; as it is confounded by data scattering (the obtained p-values are respectively 0.31, 0.13, 0.22). Interaction with the surface treatment factor is also under the significance threshold.

Conversely, the statistical tool applied to the complete 2-by-3 experimental design revealed that surface treatment does affect the fatigue response. In particular, shot-peening and subsequent machining have a positive effect with respect to the parts that underwent shot-peening only. Furthermore, swapping the orders of machining and shot-peening treatment has the capability of featuring a further beneficial effect. These increments are both significant with p-values under the commonly accepted threshold of 0.05. The same tool was used to confirm these two fatigue strength enhancements are both significant. This can be regarded as one of the most important outcomes of this study. Indeed, unlike usual procedures concerning shot-peening execution immediately following production, such as in [58], swapping the order of shot-peening and machining does have a considerably beneficial impact on strength. The swap of the post-processing steps takes advantage of the compressive residual stress state that is a consequence of shot-peening, whose positive effect is largely prevalent with respect to the slight increase of surface roughness. This assertion is going to be supported by fractography: dimples created by shot-peening are not sufficiently sharp to promote crack nucleation and propagation, as it is going to be shown in the next section. Moreover, it is worth mentioning the same conclusion was also derived for the influence of shot-peening on the fatigue strength of Maraging Steel MS1 [40] processed by DMLS.

The discussion and conclusions are also confirmed by the analysis of fatigue limits (*FLs*) in the finite life domain by the Dixon method that are presented in the bar graph in Fig. 3 (A), where 90% confidence bands are included as well. An important point in the analysis is comparison of the obtained fatigue limits for each of datasets to the corresponding *UTS* values. Considering that a *FL*/*UTS* ratio of 50% is a commonly accepted reference for metallic materials [59], 0.5·*UTS* levels are appended in the same bar graph for both untreated and heat-treated conditions. As a first point, it is worth mentioning the obtained results agree with those of the previous study [37]. In that research, vertically built, shot-peened, heat -treated and machined samples with 1 mm allowance were fatigued and related results returned a fatigue limit in the order of 39% of the corresponding *UTS*. In addition, that study highlighted a greater allowance led to the significant increase of the *FL*. PHM sample set considered in the present study followed the same AM and post-processing procedure, except for allowance that is 0.5mm in this study, instead of 1mm. The value of 32% for *FL*/*UTS*, obtained in this study, is therefore in fair agreement with the *FL/UTS* ratio of 39% obtained in the study [37].

It is worth mentioning that machining after shot-peening leads to a 10% increase of *FL/UTS* (on average, from 20% to 30%) with respect to unmachined parts, whereas, shot-peening after machining leads to a further 10% increase of *FL/UTS* (on average, from 30% to 40%). The highest *FL/UTS* ratio was obtained for Set MP, which indicates that machining with subsequent shot-peening is highly

effective and beneficial for the fatigue strength of 15-5 PH Stainless Steel regardless of heat-treatment.

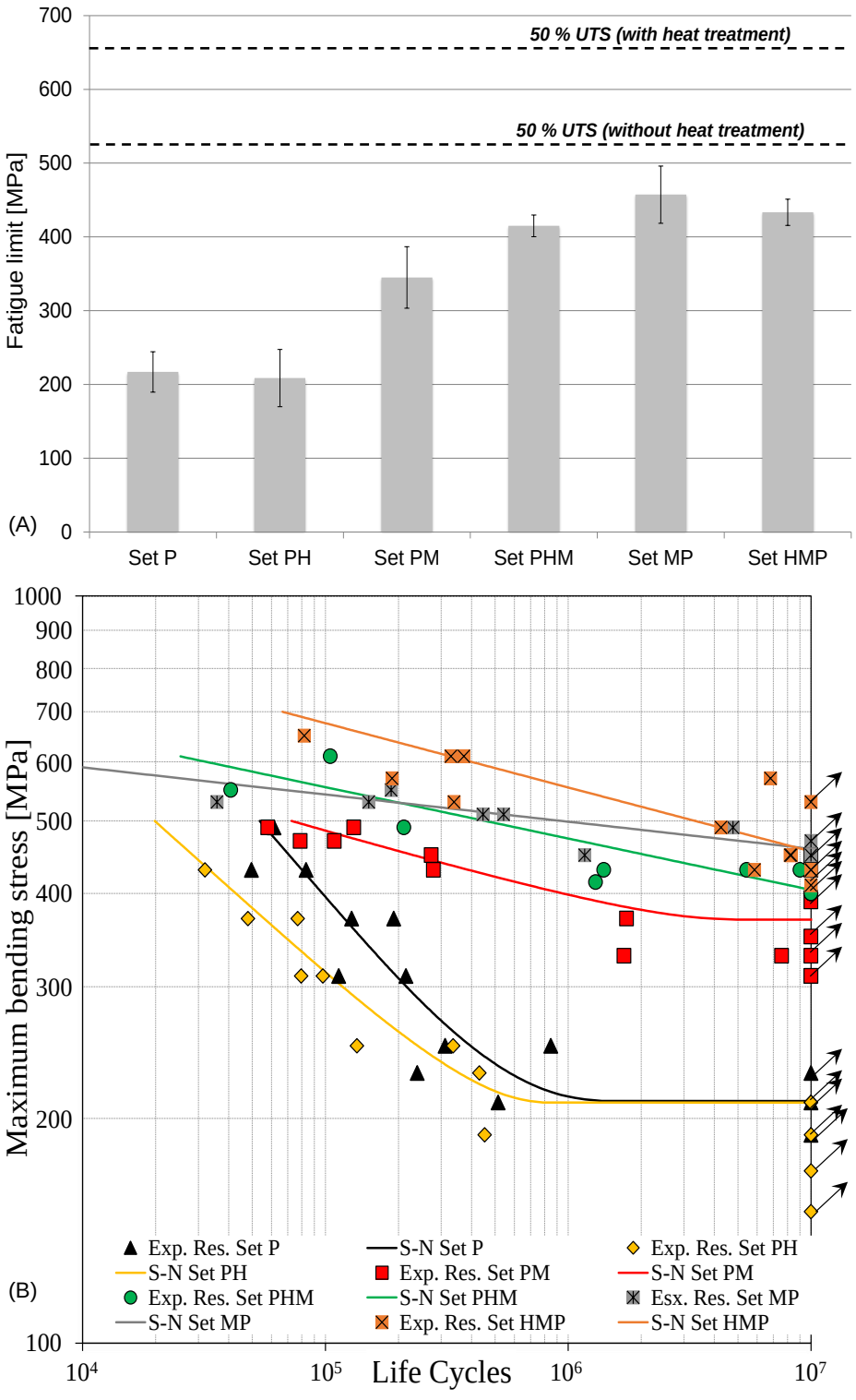

Fig. 3: (A): Fatigue limits for infinite life for the investigated Sets along with their 90% confidence bands; (B): S-N curves for the investigated Sets, processed by an MLE approach (slanted arrows indicate runouts)

A further interesting point is that the highest value of *FL/UTS*, around 44%, is close to that of wrought material, which suggests that a proper optimization of the order of post-processing steps is crucial for obtaining fatigue strengths of *AM* parts being comparable to those of conventionally produced parts. In addition, the retrieved fatigue limit for Set MP corresponds to a doubled resistance with respect to as built condition.

The *FL* analysis was accompanied by the determination of the S-N curves by the *MLE* method, that takes both not censoring (failure) and censoring (runout) data into account, thus combining the S-N relationship in the finite life domain to the fatigue strength for infinite life. These curves are plotted in Fig. 3 (B) along with experimental data including runouts (indicated by slanted arrows). It is worth mentioning that, on one hand the sloping parts are well consistent with those determined by the more conventional linear regression method that are depicted in Fig. 2. On the other hand, the horizontal trends and the fatigue strengths at runout yielded by the optimizations process are well aligned with those determined by the Dixon method and reported in Fig. 3 (A).

4.4 Micrography and fractography observations

The study was completed by micrographic and fractographic observations. Micrography (Fig. 4) enables assessment of modifications in the stacked structure by the post-processing heat treatment. Not-heat-treated samples were studied by observing sections both in the build plane and along the stacking direction. Laser scans and overlapped layers are well visible in Fig.s 4 (A, B) that show micrographic images of a sample from the set MP, which has not undergone heat-treatment. Afterwards, the analysis was performed on heat-treated samples: a picture is depicted in Fig.s 4 (C, D), which show micrographic images of a sample from Set HMP. In this case, the previously mentioned patterns are still visible, although material structure appears to be a bit more uniform as an effect of the heat-treatment. This small difference between the microstructures of heat-treated and non-heat-treated samples reflects into poor differences between the fatigue behaviour of the sample sets.

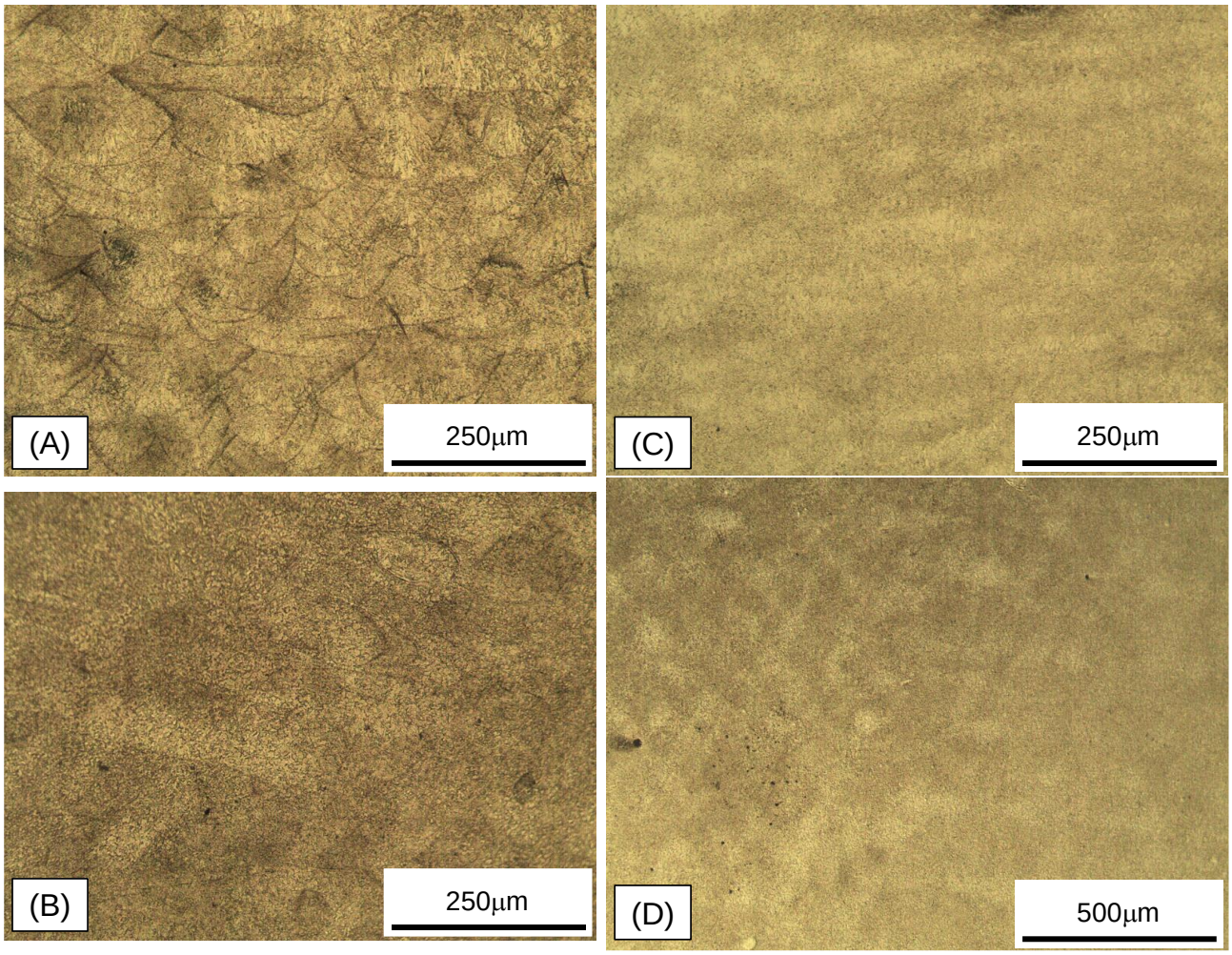

Fig. 4: Micrographies involving Sets MP and HMP: (A): MP: stacked layers observed on a longitudinal (aligned with the vertical build direction) section; (B): MP: laser scans on the build plane, observed on a cross section; (C): HMP: longitudinal (aligned with the vertical build direction) section; (D): HMP: cross section (on the build plane)

Fractographic analyses made it possible to investigate the location of nucleation points, involving unmachined, unmachined heat-treated, and machined samples. For unmachined samples, multiple crack nucleation points could be observed on the surface, which indicates that the roughness irregularities acted as crack triggers and severe notches, thus promoting crack initiation and subsequent propagation. Fig. 5 refers to Set P, whereas Fig. 6 is related to Set PH. As mentioned above, heat treatment makes material more brittle and, especially, highly notch-sensitive [33-34], which furtherly reduces the fatigue strength due to the increased number of nucleation sites.

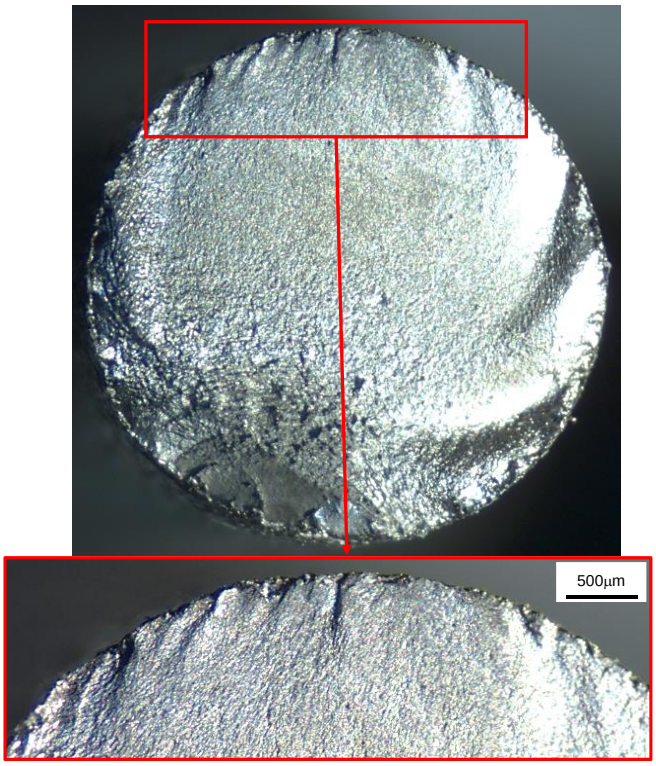

Fig. 5: Fractography involving Set P: Multiple nucleation sites (at the top of the picture) in an unmachined sample with related detail (images by stereoscopic microscope)

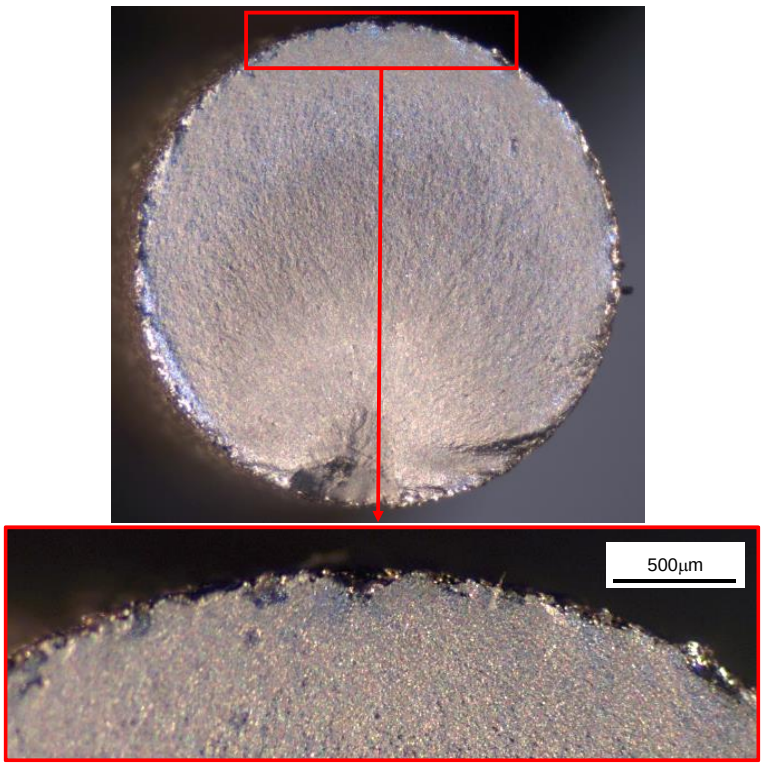

Fig. 6: Fractography involving Set PH: Multiple nucleation points are also present on the surface after heat treatment that furtherly brittles the studied material

The main features of crack initiation points were also investigated by SEM-FEG analyses. They confirmed cracks initiate from the external layers, being usually triggered by surface asperities and

porosities, where unmelted powders are usually present. These act as internal notches, thus promoting fatigue damage, which is also consistent with the remarks in other studies dealing with the same or different materials [33-34, 60-64]. For instance, a crack initiation point in a sample of Set P is shown in Fig. 7 (A), whereas Fig. 7 (B) refers to Set PH that underwent heat-treatment. Regarding the latter, close initiation points with an array of unmelted powders and fusion defects are visible.

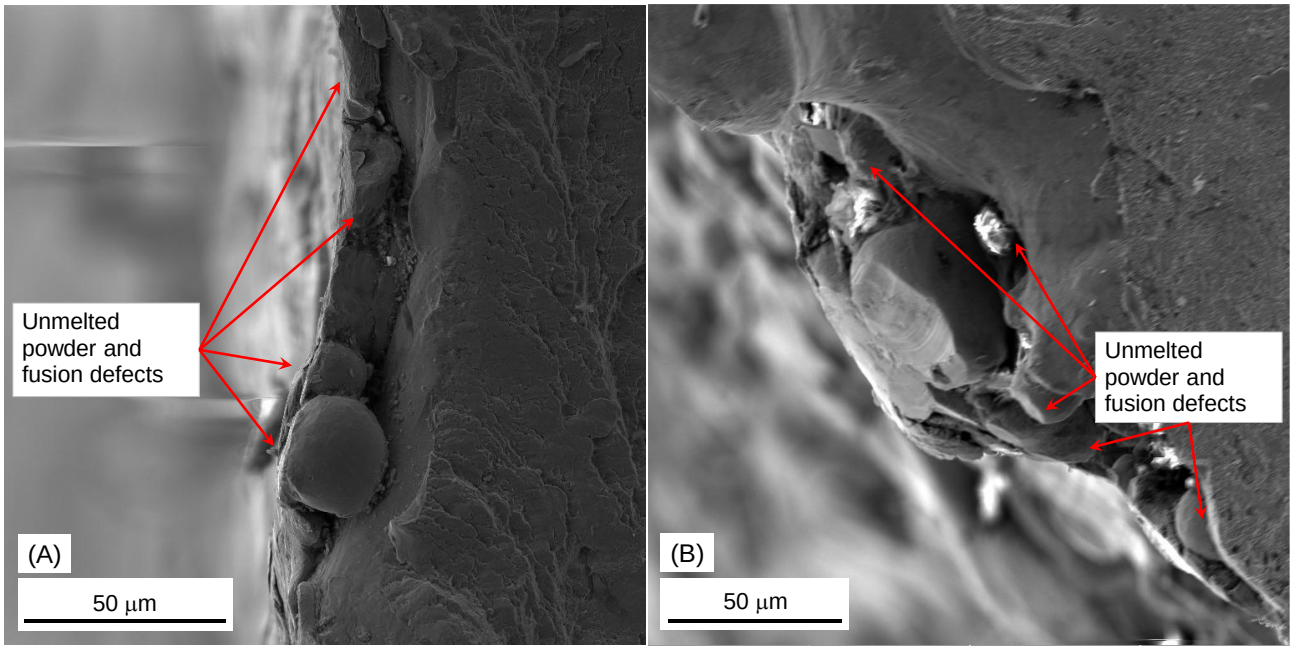

Fig. 7: SEM-FEG observations depicting crack initiation points for samples of (A) Set P; (B) Set PH

On the other hand, the beneficial effect of machining was quite evident: it made it possible to smoothen the surface, thus moving crack initiation sites from the surface to in-depth (100-150 μm from the surface) porosities. It is worth mentioning that this phenomenon was also observed in sample sets that underwent shot-peening after machining: in particular, Fig. 8 refers to Set HMP, where crack started from an internal void at 126 μm depth. Moreover, as also highlighted in [16, 37], the effect of machining is usually twofold, as it removes surface contour lines and, consequently, sub-surface (some tenths of μm) defects that are most concentrated at the interface between contour lines and internal hatch.

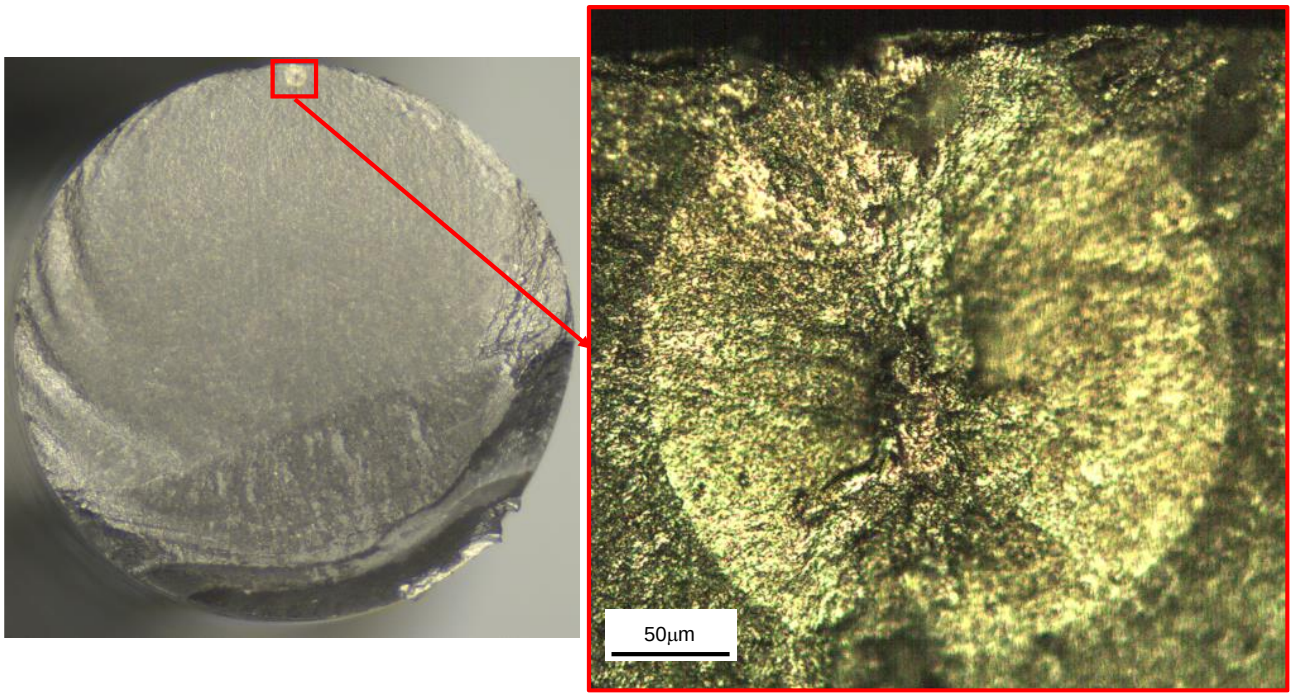

Fig. 8: Fractography involving Set HMP: A crack nucleating from a subsurface porosity (by stereoscopic microscope) with related detail (by optical microscope)

Fatigue striations in a fatigue propagation region are depicted in Fig. 9 (A) with reference to a Set P specimen: however, beachmarks appear to be the same regardless the presence of heat-treatment. The analysis of fracture morphology upon final fracture area was particularly interesting. In the case of not heat-treated parts, it revealed a completely ductile fracture with clear dimples being uniformly distributed (Fig. 9 (B)). Some spots of unmelted powder were also observed like that visible in Fig. 9 (B) that is contained in a dimple valley. When considering heat-treated components, surface morphology appeared to be generally different. In some cases, regions, where signature of ductile fracture pullout was not present at all, were observed. Therefore, the fracture mode appeared to be completely brittle like in Fig. 9 (C). In some other portions of the final fracture, some spots and some regions of ductile fracture with characteristic dimples were also observed, as it is highlighted in Fig. 9 (D). It is worth mentioning these outcomes support the previously mentioned hypothesis concerning the detrimental effect of heat-treatment under fatigue loads. When operating under cyclic loads, heat-treatment turns fracture from ductile to predominantly brittle, which is, in turn, responsible for fatigue crack initiation from surface asperities or unmelted powder spots and lowered strength. The reported outcome is basically in agreement with the results reported in [33-34], although the presence of some ductile fracture regions is a point of novelty.

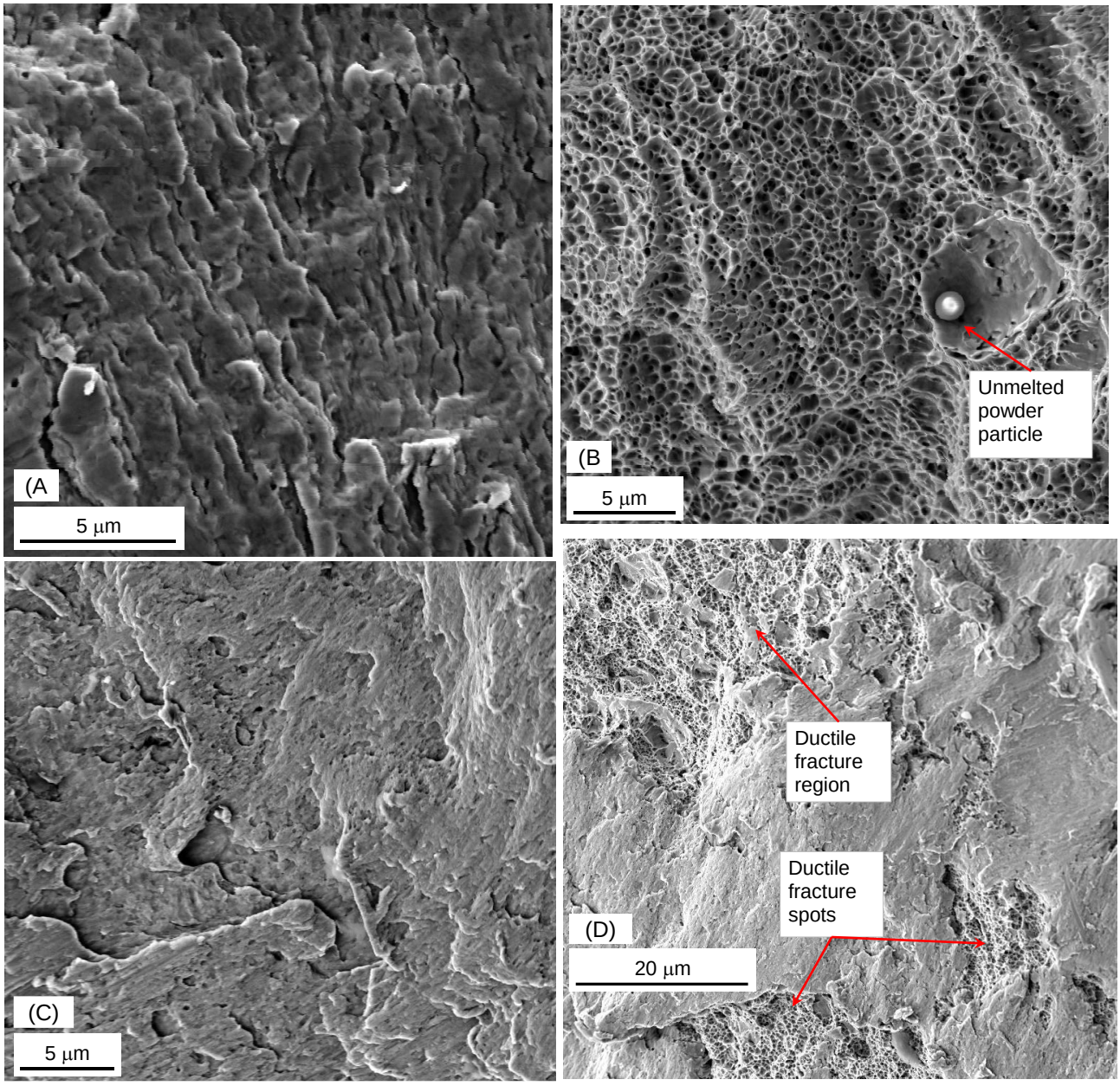

Fig. 9: SEM-FEG observations depicting (A) fatigue striations in a sample of Set P; (B) completely ductile fracture in a sample of Set P; (C) completely brittle fracture and (D) predominantly brittle fracture with some ductile fracture spots in a sample of Set PH

5. CONCLUSIONS

This study aims at filling the gap, with reference to the fatigue behaviour of 15-5 PH Stainless Steel. In particular, studies focusing on the combined effect of machining, shot-peening and heat treatment are missing. This topic has been tackled experimentally, drawing a two-factor design, taking surface

and heat-treatments into account. Fatigue tests have been run under rotary bending with the aim of determining the fatigue response in the finite life domain, as well as the fatigue limit for infinite life. For the sake of methodological rigor, all the results have been compared and interpreted by appropriate statistical tools.

Based on the obtained results, heat-treatment does not significantly affect the fatigue strength of 15-5 PH Stainless Steel. Heat-treatment effect is usually related to enduing precipitation hardening and relaxation of residual stresses generated during AM building process. However, for unmachined and shot-peened samples, its effect is even slightly detrimental, as it brittles the material, reduces beneficial compressive residual stresses yielded by shot-peening and increases notch sensitivity. For machined samples with smooth surfaces, heat-treatment leads to a small increase of fatigue strength, in the order of just a few percent. Conversely, surface treatments are remarkably beneficial for fatigue strength. Running shot-peening before machining leads to an increase of *FL/UTS* ratio around 10%, whereas, swapping the order of the surface treatment procedures, i.e., running machining before shot-peening, leads to an increase of *FL/UTS* ratio around 20%.

Surface smoothening due to machining reduces the potential surface crack initiation sites; moreover, its beneficial contribution is twofold, as it allows for removal of contour layers and of sub-surface defects at the interface with internal hatches. The rationale for running shot-peening after machining is to take advantage of beneficial compressive residual stress state induced by the shot-peening, which is removed, if machining is performed after shot-peening. The optimization of the order of surface-treatment processes leads to a *FL/UTS* ratio being close to 44%, which is almost comparable to that of wrought material and doubled with respect to as built condition.

ACKNOWLEDGEMENTS

The research presented in the paper represents a part of research carried out within the project "Advanced design rules for optimal dynamic properties of additive manufacturing products – A_MADAM". This project has received funding from the European Union's Horizon 2020 research and innovation programme under the Marie Skłodowska-Curie grant agreement No 734455: the authors wish to acknowledge the financial support by the European Commission.

The authors from Serbia (S.Ć.-K., N.B. and Z.Š.) are obliged to acknowledge the support of Ministry of Education, Science and Technology Development of Republic of Serbia to its institution through grant No. 451-03-68/2022-14/200108.

AUTHOR CONTRIBUTIONS

Conceptualization, G.O., S.Ć.-K.; Methodology, G.O., D.C.; Sample fabrication and post-processing, N.B., S.Ć.-K., Z.Š.; Experimental campaign, G.O., M.D.A, S.F., F.R.; Data statistical processing, G.O.; Data discussion, G.O.; Microscopy observations, G.O.; Paper (original version) writing, G.O.; Paper (revised version) writing, G.O.; Supervision, G.O., D.C.; Funding Acquisition (A_MADAM Project Leader), S.Ć.-K..

REFERENCES

1. Haghdadi N, Laleh M, Moyle M, Primig S. Additive manufacturing of steels: a review of achievements and challenges. *J Mater Sci*. 2021; 56(1): 64-107.
2. Huang R, Riddle M, Graziano D, Warren J, Das S, Nimbalkar, S, Cresko J, Masanet E. Energy and emissions saving potential of additive manufacturing: the case of lightweight aircraft components. *J Clean Prod*. 2016; 135: 1559-1570.
3. Fitzsimons L, McNamara G, Obeidi M, Brabazon D. The circular economy: additive manufacturing and impacts for materials processing. *Encyclopedia of Renewable and Sustainable Materials*. 2020; 1: 81-92.
4. Bhuvanesh Kumar M, Sathiya P. Methods and materials for additive manufacturing: A critical review on advancements and challenges. *Thin-Walled Struct*. 2021; 159.
5. Santa-Aho S, Kiviluoma M, Jokiaho T, Gundgire T, Honkanen M, Lindgren M, Vippola M. Additive manufactured 316l stainless-steel samples: Microstructure, residual stress and corrosion characteristics after post-processing. *Metals*. 2021; 11(2): 1-16.
6. Braun M, Mayer E, Kryukov I, Wolf C, Böhm S, Taghipour A, Wu RE, Ehlers S, Sheikhi S. Fatigue strength of PBF-LB/M and wrought 316L stainless steel: effect of post-treatment and cyclic mean stress. *Fatigue Fract Eng Mater Struct*. 2021; 1-17.
7. Nezhadfar PD, Shamsaei N, Phan N. Enhancing ductility and fatigue strength of additively manufactured metallic materials by preheating the build platform. *Fatigue Fract Eng Mater Struct*. 2021; 44: 257-270.
8. Sun Z, Tan X, Tor SB, Chua CK Simultaneously enhanced strength and ductility for 3D-printed stainless steel 316L by selective laser melting. *NPG Asia Mater*. 2018; 10(4):127-136.
9. Riemer A, Leuders S, Thöne M, Richard HA, Tröster T, Niendorf T. On the fatigue crack growth behavior in 316L stainless steel manufactured by selective laser melting. *Eng Fract Mech*. 2014; 120: 15-25.
10. McGuire MF. *Stainless steels for design engineers*. ASM International, Cleveland; 2008.
11. Erlach SD, Leitner H, Bischof M, Clemens H, Danoix F, Lemarchand D, et al. Comparison of NiAl precipitation in a medium carbon secondary hardening steel and C-free PH13-8 maraging steel. *Mater Sci Eng A*. 2006; 429(1-2): 96-106.
12. Asgari H, Mohammadi M. Microstructure and mechanical properties of stainless steel CX manufactured by Direct Metal Laser Sintering. *Mater Sci Eng A*. 2018; 709: 82-89.
13. Guo Z, Sha W, Vaumousse D. Microstructural evolution in a PH13-8 stainless steel after ageing. *Acta Mater*. 2003; 51(1): 101-116.
14. Hadadzadeh A, Shahriari A, Amirkhiz BS, Li J, Mohammadi M. Additive manufacturing of an Fe–Cr–Ni–Al maraging stainless steel: Microstructure evolution, heat treatment, and strengthening mechanisms. *Mater Sci Eng A*. 2020; 787: 139470.

15. Chang C, Yan X, Bolot R, et al. Influence of post-heat treatments on the mechanical properties of CX stainless steel fabricated by selective laser melting. *J Mater Sci*. 2020; 55 (19): 8303-8316.
16. Ćirić-Kostić S, Croccolo D, De Agostinis M, Fini S, Olmi G, Paiardini L, et al. Fatigue response of additively manufactured Maraging Stainless Steel CX and effects of heat treatment and surface finishing. *Fatigue Fract Eng Mater Struct*. 2022; 45(2): 482-499.
17. Abe, Y., Kurose, T., Santos, M. V. A., Kanaya, Y., Ishigami, A., Tanaka, S., & Ito, H. Effect of layer directions on internal structures and tensile properties of 17-4ph stainless steel parts fabricated by fused deposition of metals. *Materials*. 2021; 14(2), 1-12.
18. Lin X., Cao Y., Wu X., Yang H., Chen J, Huang W. Microstructure and mechanical properties of laser forming repaired 17-4PH stainless steel. *Mater Sci Eng A*. 2012; 553: 80-88.
19. Wang Y, Tan Q, Pu F, Boone D, Zhang M. A review of the application of additive manufacturing in prosthetic and orthotic clinics from a biomechanical perspective. *Engineering*. 2020; 6(11): 1258-1266.
20. Committee AH. *ASM Handbook Volume 4 Heat Treating*. ASM Standards. American Society for Metals, Materials Park, 1991.
21. Yadollahi A, Mahmoudi M, Elwany A, Doude H, Bian L, Newman Jr JC. Fatigue-life prediction of additively manufactured material: Effects of heat treatment and build orientation. *Fatigue Fract Eng Mater Struct*. 2020; 43: 831–844.
22. Rafi HK, Starr TL, Stucker BE. A comparison of the tensile, fatigue, and fracture behavior of ti-6Al-4V and 15-5 PH stainless steel parts made by selective laser melting. *Int J Adv Manuf Technol*. 2013; 69(5-8): 1299-1309.
23. Abdelshehid M, Mahmodieh K, Mori K, Chen L, Stoyanov P, Davlantes D, et al. On the correlation between fracture toughness and precipitation hardening heat treatments in 15-5PH Stainless Steel. *Eng Fail Anal*. 2007; 14(4): 626-631.
24. Sarkar S, Kumar CS, Nath AK. Effects of different surface modifications on the fatigue life of selective laser melted 15–5 PH stainless steel. *Mater Sci Eng A*. 2019; 762.
25. Roberts D, Zhang Y, Charit I, Zhang J. A comparative study of microstructure and high-temperature mechanical properties of 15-5 PH stainless steel processed via additive manufacturing and traditional manufacturing. *Prog Addit Manuf*. 2018: 3(3): 183-190.
26. Rafi HK, Starr TL, Stucker BE. A comparison of the tensile, fatigue, and fracture behavior of Ti–6Al–4V and 15–5 PH stainless steel parts made by selective laser melting. *Int J Adv Manuf Technol*. 2013; 69(5-8): 1299-1309.
27. Sagar S, Zhang Y, Wu L, Park H-Y, Lee J-H, Jung Y-G, Zhang J. Room-temperature charpy impact property of 3d-printed 15–5 stainless steel. *J Mater Eng Perform*. 2018; 27(1): 52-56.
28. Huang E-W, Lee SY, Jain J, Tong Y, An K, Tsou N-T, et al. Hardening steels by the generation of transient phase using additive manufacturing. *Intermet*. 2019; 109: 60-67.
29. Ramadas H, Sarkar S, Nath AK. Three-body dry abrasive wear properties of 15–5 precipitation hardening stainless steel produced by laser powder bed fusion process. *Wear*. 2021; 470-471.
30. Sarkar S, Mukherjee S, Kumar CS, Kumar Nath A. Effects of heat treatment on microstructure, mechanical and corrosion properties of 15-5 PH stainless steel parts built by selective laser melting process. *J Manuf Process*. 2020; 50, 279-294.
31. Sagar S, Zhang Y, Choi H-H, Jung Y-G, Zhang J. Temperature-dependent Charpy impact property of 3D printed 15-5 PH stainless steel. *Mater Sci Technol*. 2021; 37(2): 190-201.

32. Lee J-R, Lee M-S, Chae H, Lee SY, Na T, Kim W-S, et al. Effects of building direction and heat treatment on the local mechanical properties of direct metal laser sintered 15-5 PH stainless steel. *Mater Charact*. 2020; 167.
33. Sarkar S, Kumar CS, Nath AK. Effects of heat treatment and build orientations on the fatigue life of selective laser melted 15-5 PH stainless steel. *Mater Sci Eng A*. 2019; 755, 235-245.
34. Sarkar S, Kumar CS, Nath AK. Effect of different heat treatments on mechanical properties of laser sintered additive manufactured parts. *J Manuf Sci Eng Trans ASME*. 2017; 139(11): 111010-1.
35. Spierings AB, Starr TL, Wegener K. Fatigue performance of additive manufactured metallic parts. *Rapid Prototyp J*. 2013; 19: 88-94.
36. Sarkar S, Kumar CS, Nath AK. Effects of different surface modifications on the fatigue life of selective laser melted 15–5 PH stainless steel. *Mater Sci Eng A*. 2019; 762: 138109.
37. Croccolo D, De Agostinis M, Fini S, Olmi G, Bogojevic N, Ciric-Kostic S. Effects of build orientation and thickness of allowance on the fatigue behaviour of 15–5 PH stainless steel manufactured by DMLS. *Fatigue Fract Eng Mater Struct*. 2018; 41(4): 900-916.
38. Croccolo D, De Agostinis M, Fini S, Olmi G, Vranic A, Ciric-Kostic S. Influence of the build orientation on the fatigue strength of EOS maraging steel produced by additive metal machine. *Fatigue Fract Eng Mater Struct*. 2016; 39(5): 637-647.
39. Croccolo D, De Agostinis M, Fini S, Olmi G, Robusto F, Ćirić-Kostić S, Moraca S, Bogojević N. Sensitivity of direct metal laser sintering maraging steel fatigue strength to build orientation and allowance for machining. *Fatigue Fract Eng Mater Struct*. 2019; 42(1): 374-386.
40. Croccolo D, De Agostinis M, Fini S, Olmi G, Robusto F, Ćirić-Kostić S, Vranic A, Bogojević, N. Fatigue response of as-built DMLS maraging steel and effects of aging, machining, and peening treatments. *Metals*. 2018; 8(7): 505.
41. International Organization for Standardization ISO 1143:2010. *Standard - Metallic materials - Rotating bar bending fatigue testing*. Geneva, Switzerland: International Organization for Standardization (ISO); 2010.
42. https://www.eos.info/material-m.
43. ASTM E18-16. Standard Test Methods for Rockwell Hardness of Metallic Materials. West Conshohocken, PA, United States: ASTM International; 2016.
44. International Organization for Standardization ISO 12107:2012. *Metallic Materials – Fatigue Testing – Statistical Planning and Analysis of Data*. Geneva, Switzerland: International Organization for Standardization (ISO); 2012.
45. Pascual FG, Meeker WQ. Estimating fatigue curves with the random fatigue-limit model. *Technometrics* 1999; 41: 277-289.
46. Pollak RD, Palazotto AN. A comparison of maximum likelihood models for fatigue strength characterization in materials exhibiting a fatigue limit. Probabilistic Eng. Mech. 2009; 24: 236-241.
47. Strzelecki P, Tomaszewski T, Sempruch J. A method for determining a complete S-N curve using maximum likelihood. *Proceedings of the 22nd International Conference Engineering Mechanics*. 2016, Svratka, Czech Republic, 9-12 May 2016.
48. Loren S, Lundstrom M. Modelling curved S–N curves. *Fatigue Fract Eng Mater Struct*. 2005; 28: 437-443.
49. Paolino DS, Chiandussi G, Rossetto M. A unified statistical model for S–N fatigue curves: probabilistic definition. *Fatigue Fract. Eng. Mater. Struct.* 2013; 36: 187-201.
50. Olmi G, Freddi A. A new method for modelling the support effect under rotating bending fatigue: application to Ti-6Al-4V alloy, with and without shot peening. *Fatigue Fract Eng Mater Struct*. 2013; 36(10): 981-993.
51. Dixon WJ, Massey F Jr. *Introduction to Statistical Analysis*. New York, United States: McGraw-Hill; 1983.

52. Olmi G, Comandini M, Freddi A. Fatigue on shot-peened gears: experimentation, simulation and sensitivity analyses. *Strain*. 2010; 46(4): 382-395.
53. Van Hooreweder B, Moens D, Boonen R, Sas P. The critical distance theory for fatigue analysis of notched aluminium samples subjected to repeated bending. *Fatigue Fract Eng Mater Struct*. 2012; 35: 878-884.
54. Olmi G. Low cycle fatigue experiments on Turbogenerator steels and a new method for defining confidence bands. *J Test Eval*. 2012; 40: 4, JTE104548.
55. Berger PD, Maurer RE. Experimental design with applications in management, engineering and the sciences; Duxbury Press: Belmont, CA, 2002.
56. Montgomery DC. Design and Analysis of Experiments; Wiley: New York, 2001.
57. Bhadeshia H, Honeycombe R. Steels: microstructure and properties. Butterworth-Heinemann, Oxford; 2017.
58. Sanz C, Garcia Navas V, Gonzalo O, Vansteenkiste G. Study of surface integrity of rapid manufacturing parts after different thermal and finishing treatments. *1st CIRP Conference on Surface Integrity proceedings*. 2011; 19: 294-299.
59. Niemann G, Winter H, Hohn BR. Maschinenelemente. Berlin, Germany: Springer-Verlag; 2005.
60. Garcias JF., Martins RF, Branco R, Marciniak Z, Macek W, Pereira C, Santos C. Quasistatic and fatigue behavior of an AISI H13 steel obtained by additive manufacturing and conventional method. *Fatigue Fract Eng Mater Struct*. 2021 44, 3384-3398.
61. Peng X, Wu S, Qian W, Bao J, Hu Y, Zhan Z, Guo G, Withers PJ. The potency of defects on fatigue of additively manufactured metals. *Int. J. Mech. Sci.* 2022; 221: 107185.
62. Molaei R. Fatigue and Fracture of Additively Manufactured Metallic Materials. Reference Module in Materials Science and Materials Engineering, 2021.
63. Macek W, Martins RF, Branco R, Marciniak Z, Szala M, Wroński S. Fatigue fracture morphology of AISI H13 steel obtained by additive manufacturing. *Int. J. Fract.* 2022; 235: 79-98.
64. Lee S, Rasoolian B, Silva DF, Pegues JW, Shamsaei N. Surface roughness parameter and modeling for fatigue behavior of additive manufactured parts: A non-destructive data-driven approach. *Addit. Manuf.* 2021; 46: 102094.

Highlights

1. Statistical and microscopy analyses have supported fatigue response investigation.

2. Heat-treatment increases notch sensitivity and turns fracture from ductile to brittle.

3. Shot-peening before machining has a positive impact on the fatigue strength.

4. Shot-peening after machining leads to a furtherly increased fatigue strength.